

Asymptotic results for a barrier potential model

DAVID A. EDWARDS and CHRISTOPHER S. RAYMOND

Department of Mathematical Sciences, University of Delaware, Newark, DE, USA
email: dedwards@udel.edu, craymond@udel.edu

(Received 9 June 2014; revised 16 April 2015; accepted 17 April 2015; first published online 15 May 2015)

An enhanced understanding of the microstructure of oxide ceramics will help scientists and engineers improve their efficiency and design. A phase-field model for the composition and phase distribution of the oxide ceramic components is studied. The model, which includes an obstacle in the phase portion of the energy potential, results in a minimisation problem that characterises the distribution of the bulk phases. The transition region between them is studied in several mathematically plausible asymptotic limits. The behaviour of the system in these limits provides insights into the applicability of the model and indicates appropriate parameter regimes.

Key words: Phase-field model; Asymptotics; Oxide ceramics

1 Introduction

In recent years, the use of oxide ceramics in industrial applications has exploded. Oxide ceramics are now commonly used for heat shields [4], catalysis [6], and high-intensity discharge lamps [9]. This manuscript was motivated by the use of oxide ceramics in filtration applications. Ceramic media is now used for water filtration [2], diesel particulate filtration [7], and gas filtration [8].

In order to design more efficient filters, it is useful to understand microstructure evolution in oxide ceramics. When formulating oxide ceramics, one wishes to keep track of the composition and the phase distribution of the resulting structures. Though not a precise definition, for the purposes of this manuscript, we consider the composition at position $\tilde{\mathbf{x}}$ to be the ensemble of *neutral moieties* at $\tilde{\mathbf{x}}$. For instance, such a ceramic may be composed of silicon dioxide (SiO_2) and alumina (Al_2O_3). Here, phases can represent states of matter (melt, solid) or types of crystalline structure (quartz and crystalobite for silicon dioxide, for instance).

For the purpose of this manuscript, we consider a two-phase binary alloy problem. In order to track the composition and phase distribution, we use the phase-field model of Wheeler, Boettinger, and McFadden [10, 11], extending it to a fully-infinite bulk domain through a simple transformation. The mathematical problem then reduces to minimising the free energy over all possible configurations.

We then introduce an obstacle (infinite barrier, as in [1]) in the phase portion of the energy potential. This ensures that the phase variables remain in the proper range.

The barrier potential introduces several complications into the minimisation problem. In particular, the domain splits into two bulk phases and a transition phase. We examine this transition phase in two asymptotic limits: a large barrier in the phase potential between the minima corresponding to the two bulk phases, and large concavity in one of the energy potentials for the concentration. In each case, we provide results for the concentration and the phase distribution in both the bulk regions and the transition region between them. These asymptotic results compare favourably to numerical simulations. The character of these results allows us to draw conclusions about the appropriateness of using these limits in modelling physically realisable systems.

2 Governing equations: general considerations

As described above, we wish to track the composition and phase distribution of the alloy. We denote the molar fraction of component i by

$$c_i(\tilde{\mathbf{x}}), \quad i = 1, 2, \dots, N. \quad (2.1)$$

(Note that, we will index components by Roman symbols.) As these are all molar fractions, we have that

$$\sum_{i=1}^N c_i(\tilde{\mathbf{x}}) = 1, \quad (2.2)$$

and hence we need consider only $N - 1$ independent variables c_i for any problem, since c_N can trivially be obtained by (2.2).

We consider the phase distribution at position $\tilde{\mathbf{x}}$ to be the ensemble of different phases at position $\tilde{\mathbf{x}}$. Each phase α is tracked through an order parameter

$$\phi_\alpha(\tilde{\mathbf{x}}), \quad \alpha = 1, 2, \dots, M; \quad 0 \leq \phi_\alpha \leq 1, \quad (2.3)$$

which represents the fraction of the ceramic that is in phase α . (Note that, we will index phases by Greek symbols.) For this reason, an equation analogous to (2.2) holds:

$$\sum_{\alpha=1}^M \phi_\alpha(\tilde{\mathbf{x}}) = 1, \quad (2.4)$$

and so similarly we need to consider only $M - 1$ phase variables.

Therefore, at any position $\tilde{\mathbf{x}}$ there are N different values of the compositions and M different values of the phases. To obtain the molar fraction of composition i in phase α , we just take the product $\phi_\alpha c_i$. However, in a general system there will be MN such combinations, while the present model has only $M + N$ variables. The paradox can be explained by noting that since there is a single value of ϕ_α for the *entire* system, this model implies that each component has the same division between phases. In practice, that is not true: under certain conditions, silicon dioxide may be much more likely to be in the crystal form than alumina. Other more complicated models [5] address this discrepancy.

The equilibrium configuration of the ceramic must minimise the free energy of the system, which consists of the following parts (for more details, see [3, 10, 11]):

(1) A bulk energy term

$$\tilde{f}(\vec{c}, \vec{\phi}), \quad \vec{c} = (c_1, c_2, \dots, c_{N-1}), \quad \vec{\phi} = (\phi_1, \phi_2, \dots, \phi_{M-1}). \quad (2.5)$$

For any particular alloy, the particular form of the bulk energy term $\tilde{f}(\vec{c}, \vec{\phi})$ must be specified and will be discussed later.

(2) A term

$$\frac{1}{2} \sum_{i=1}^{N-1} \sum_{j=1}^{N-1} \tilde{\kappa}_{ij} (\tilde{\nabla} c_i) \cdot (\tilde{\nabla} c_j), \quad (2.6)$$

which penalises gradients in the compositions. Here the $\tilde{\kappa}_{ij}$ are the gradient energy coefficients associated with the compositions, and they form the entries of a positive definite matrix. In their earlier work, Wheeler *et al.* [10] proposed a similar free energy functional that did not include this term. They then argued in later work [11] that inclusion of the gradient energy in composition is appropriate, especially for the case of rapid solidification where the length scale of the solute boundary layers at a moving interface may approach atomic dimensions.

(3) A term

$$\frac{1}{2} \sum_{\alpha=1}^{M-1} \sum_{\beta=1}^{M-1} \tilde{\lambda}_{\alpha\beta} (\tilde{\nabla} \phi_{\alpha}) \cdot (\tilde{\nabla} \phi_{\beta}), \quad (2.7)$$

which plays a similar role, but penalises gradients in the phases. Here the $\tilde{\lambda}_{\alpha\beta}$ are the gradient energy coefficients associated with the phases, and they also form the entries of a positive definite matrix.

In [11] Wheeler, Boettinger and McFadden then use the components of the free energy discussed above to analyse a free energy functional. In our multi-component context, this functional would be of the form

$$\tilde{\mathcal{F}}[\vec{c}, \vec{\phi}] = \int_{\tilde{V}} \tilde{f}(\vec{c}, \vec{\phi}) + \frac{1}{2} \sum_{i=1}^{N-1} \sum_{j=1}^{N-1} \tilde{\kappa}_{ij} (\tilde{\nabla} c_i) \cdot (\tilde{\nabla} c_j) + \frac{1}{2} \sum_{\alpha=1}^{M-1} \sum_{\beta=1}^{M-1} \tilde{\lambda}_{\alpha\beta} (\tilde{\nabla} \phi_{\alpha}) \cdot (\tilde{\nabla} \phi_{\beta}) d\tilde{V}. \quad (2.8)$$

We specialise to the one-dimensional case with $M = N = 2$, in which case we can drop the subscripts on c and ϕ since $c_2 = 1 - c_1$, etc. For later computational simplicity, we wish to take the domain as fully infinite. As $\tilde{x} \rightarrow \pm\infty$, we recover the two pure phases:

$$\phi(-\infty) = 1, \quad \phi(\infty) = 0, \quad (2.9)$$

while the concentrations approach constants

$$c(-\infty) = c_-, \quad c(\infty) = c_+, \quad (2.10)$$

which must be determined. [The choice of phase is arbitrary, so we could have just as easily reversed the 0 and 1 in (2.9).]

It can be shown in physically reasonable cases that either $\tilde{f}(c_-, 1)$ or $\tilde{f}(c_+, 0)$ is nonzero [for instance, see (3.6) below]. Therefore, the free energy as defined in (2.8) will be

unbounded. Hence, we redefine the free energy density as an average:

$$\tilde{\mathcal{F}}[c, \phi] = \lim_{\tilde{L} \rightarrow \infty} \frac{1}{2\tilde{L}} \int_{-\tilde{L}}^{\tilde{L}} \tilde{F} \left(c, \phi, \frac{dc}{d\tilde{x}}, \frac{d\phi}{d\tilde{x}} \right) d\tilde{x}, \quad (2.11a)$$

$$\tilde{F} \left(c, \phi, \frac{dc}{d\tilde{x}}, \frac{d\phi}{d\tilde{x}} \right) = \tilde{f}(c, \phi) + \frac{\tilde{\kappa}}{2} \left(\frac{dc}{d\tilde{x}} \right)^2 + \frac{\tilde{\lambda}}{2} \left(\frac{d\phi}{d\tilde{x}} \right)^2. \quad (2.11b)$$

Thus, our problem reduces to a standard calculus-of-variations minimisation problem for the free energy. From conservation of mass, we have that

$$\lim_{\tilde{L} \rightarrow \infty} \frac{1}{2\tilde{L}} \int_{-\tilde{L}}^{\tilde{L}} c d\tilde{x} = \bar{c}, \quad (2.12)$$

where \bar{c} is an average value of c determined at the beginning of the experiment.

Minimising subject to this constraint is equivalent to minimising

$$\tilde{\mathcal{G}}[c, \phi] = \lim_{\tilde{L} \rightarrow \infty} \frac{1}{2\tilde{L}} \int_{-\tilde{L}}^{\tilde{L}} \tilde{F} - \tilde{\mu}c d\tilde{x},$$

where $\tilde{\mu}$ is a Lagrange multiplier. Performing the standard analysis, we obtain

$$\frac{\delta \tilde{\mathcal{G}}}{\delta c} = \lim_{\tilde{L} \rightarrow \infty} \frac{1}{2\tilde{L}} \left\{ \left[\psi \tilde{\kappa} \frac{dc}{d\tilde{x}} \right]_{-L}^L + \int_{-L}^L \psi \left(\frac{\partial \tilde{f}}{\partial c} - \tilde{\mu} - \tilde{\kappa} \frac{d^2c}{d\tilde{x}^2} \right) d\tilde{x} \right\} = 0,$$

where ψ is a test function. (Note that given the form of $\tilde{\mathcal{G}}$, a suitable test function can approach a nonzero constant as $|\tilde{x}|$ gets large.) Hence, we have

$$\frac{\partial \tilde{f}}{\partial c} - \tilde{\kappa} \frac{d^2c}{d\tilde{x}^2} = \tilde{\mu}, \quad (2.13a)$$

$$\frac{dc}{d\tilde{x}}(\pm\infty) = 0. \quad (2.13b)$$

Equation (2.13a) also results from the analysis in Cogswell and Carter [3], where $\tilde{\mu}$ is related to a normalised version of the difference of the chemical potentials corresponding to each composition. Equation (2.13b) is consistent with our statement in (2.10); we note that the second derivative will also vanish as $\tilde{x} \rightarrow \pm\infty$. Thus, we obtain the following:

$$\frac{\partial \tilde{f}}{\partial c}(0, c_+) = \frac{\partial \tilde{f}}{\partial c}(1, c_-) = \tilde{\mu}. \quad (2.14)$$

Considering $\delta \tilde{\mathcal{G}}/\delta \phi$, the constraint does not come into play and we obtain

$$\frac{\partial \tilde{f}}{\partial \phi} - \tilde{\lambda} \frac{d^2\phi}{d\tilde{x}^2} = 0, \quad (2.15a)$$

$$\frac{d\phi}{d\tilde{x}}(\pm\infty) = 0. \quad (2.15b)$$

Multiplying (2.13a) by $dc/d\tilde{x}$ and equation (2.15a) by $d\phi/d\tilde{x}$ and manipulating the sum

of the results, we obtain an expression that can be integrated once to yield the following:

$$\tilde{\mu}c - \tilde{f}(\phi, c) + \frac{1}{2}\tilde{\lambda} \left(\frac{d\phi}{d\tilde{x}}\right)^2 + \frac{1}{2}\tilde{\kappa} \left(\frac{dc}{d\tilde{x}}\right)^2 = H, \tag{2.16}$$

where H is a constant. In particular, if we substitute $\tilde{x} = \pm\infty$ into (2.16), we obtain

$$\tilde{\mu}c_- - \tilde{f}(1, c_-) = \tilde{\mu}c_+ - \tilde{f}(0, c_+). \tag{2.17}$$

Solving (2.17) for $\tilde{\mu}$ and combining with (2.14), we have

$$\frac{\partial\tilde{f}}{\partial c}(0, c_+) = \frac{\partial\tilde{f}}{\partial c}(1, c_-) = \frac{\tilde{f}(0, c_+) - \tilde{f}(1, c_-)}{c_+ - c_-} = \tilde{\mu}, \tag{2.18}$$

which is the *common tangent* constraint. Essentially, it says that the secant line connecting the values of \tilde{f} corresponding to the two bulk phases must be parallel to the tangent lines to \tilde{f} at each of the two bulk phases.

3 The barrier potential

We now specialise the general results from Section 2 to the case we wish to study. First, we assume that \tilde{f} consists of the following two parts:

(1) A term

$$\sum_{\alpha=1}^M \phi_{\alpha} \tilde{G}_{\alpha}(\vec{c}), \quad \vec{c} = (c_1, c_2, \dots, c_{N-1}), \tag{3.1}$$

which is the sum of the bulk free energy density $\tilde{G}_{\alpha}(\vec{c})$ of phase α , weighted by the order parameter ϕ_{α} .

(2) A term

$$\tilde{U}(\vec{\phi}), \quad \vec{\phi} = (\phi_1, \phi_2, \dots, \phi_{M-1}), \tag{3.2}$$

which measures the energy potential associated with the phase.

We again specialise to the one-dimensional case with $M = N = 2$. The true forms of the \tilde{G}_{α} can be quite complicated, but since we are interested at examining the situation where they are near their minima, for our purposes they can be approximated as quadratics:

$$\tilde{G}_{\alpha}(c) = \tilde{G}_{\alpha}^* + \frac{\tilde{h}_{\alpha}^2(c - c_{\alpha}^*)^2}{2}, \quad \tilde{h}_{\alpha} > 0, \tag{3.3}$$

where c_{α}^* is the minimum value for the bulk free energy density for phase α .

Typically, away from a thin interface one would normally see the phases in pure form; hence, local energy minimisers of $U(\phi)$ should be $\phi = 0$ and $\phi = 1$, corresponding to the two pure phases. Moreover, given our interpretation of ϕ as a phase, we want to force ϕ to be bounded between 0 and 1. One approach is to put an infinite barrier at those values to keep ϕ trapped in that range:

$$\tilde{U}(\phi) = \tilde{W}U(\phi), \quad U(\phi) = \begin{cases} \phi(1 - \phi), & 0 \leq \phi \leq 1, \\ \infty, & \text{else,} \end{cases} \tag{3.4}$$

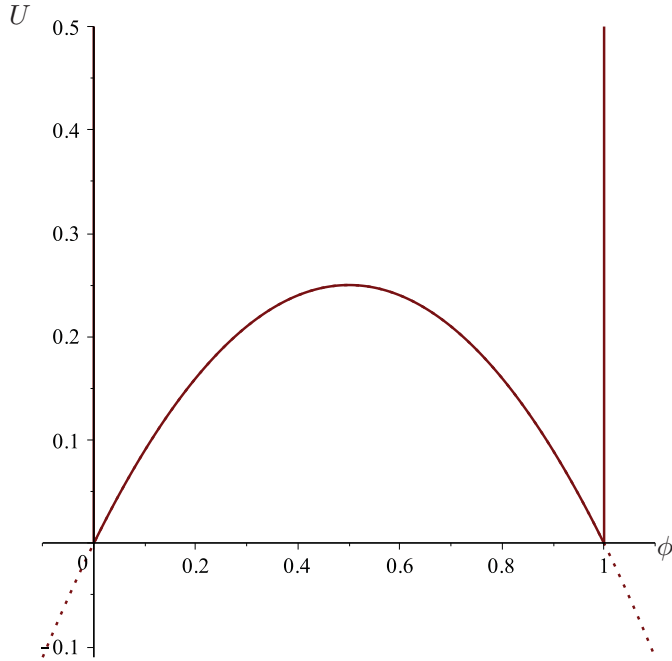


FIGURE 1. U with (solid) and without (dotted) barrier.

as shown in the solid line in Figure 1. Here, \tilde{W} measures the size of the internal maximum in the potential. Note from (3.4) that U is defined all the way to the endpoints of the interval, as will be needed for later analysis.

The form of (3.4) can be thought of as the limit of some smooth potential $U_\epsilon(\phi)$ as some small parameter $\epsilon \rightarrow 0$. Some examples are

$$U_\epsilon(\phi) = \phi(1 - \phi) + \frac{\epsilon}{\phi(1 - \phi)}, \quad U_\epsilon(\phi) = \phi(1 - \phi) - \log(\phi(1 - \phi)/\epsilon), \quad (3.5a)$$

$$U_\epsilon(\phi) = \phi(1 - \phi) + \exp\left(\frac{\epsilon}{\phi(1 - \phi)}\right). \quad (3.5b)$$

However, in addition to the algebraic simplicity provided by (3.4), there is an additional physical advantage as well. In certain applications (beyond the scope of this manuscript), it is common to apply an outside energy field which is linear in ϕ . This will shift the positions of the minima, as long as the potential is smooth. Hence by choosing a potential of the form (3.4), we can always keep the minima pinned at $\phi = 0$ and 1.

With these assumptions, we have

$$\tilde{f}(c, \phi) = \phi \left[\tilde{G}_1^* + \frac{\tilde{h}_1^2(c - c_1^*)^2}{2} \right] + (1 - \phi) \left[\tilde{G}_2^* + \frac{\tilde{h}_2^2(c - c_2^*)^2}{2} \right] + \tilde{W}U(\phi). \quad (3.6)$$

We now scale our problem to introduce dimensionless variables and parameters. We scale the bulk free energy densities by the difference between their minima:

$$G_x(c) = \frac{\tilde{G}_x(c) - \tilde{G}_1^*}{\Delta\tilde{G}}, \quad \Delta\tilde{G} = \tilde{G}_2^* - \tilde{G}_1^*. \tag{3.7}$$

(This is obviously not the only choice; we could just have easily chosen the sum of the minima. However, the choice does not appreciably affect our subsequent work.) Substituting (3.7) into (3.3) yields the functional forms

$$G_1(c) = \frac{h_1^2(c - c_1^*)^2}{2}, \quad h_1^2 = \frac{\tilde{h}_1^2}{\Delta\tilde{G}}, \tag{3.8a}$$

$$G_2(c) = 1 + \frac{h_2^2(c - c_2^*)^2}{2}, \quad h_2^2 = \frac{\tilde{h}_2^2}{\Delta\tilde{G}}. \tag{3.8b}$$

Since there is no experimental length scale for the problem, we must choose a scale including $\tilde{\kappa}$, \tilde{W} , or $\tilde{\lambda}$. We choose the first:

$$x = \tilde{x} \sqrt{\frac{\Delta\tilde{G}}{\tilde{\kappa}}}. \tag{3.9}$$

Substituting (3.4), (3.7), and (3.9) into (3.6), we have the following:

$$f(c, \phi) = \frac{\tilde{f}(c, \phi)}{\Delta\tilde{G}} = \phi G_1(c) + (1 - \phi)G_2(c) + WU(\phi) + \frac{\tilde{G}_1^*}{\Delta\tilde{G}}, \tag{3.10a}$$

$$W = \frac{\tilde{W}}{\Delta\tilde{G}}, \quad \lambda = \frac{\tilde{\lambda}}{\tilde{\kappa}}. \tag{3.10b}$$

The last term in (3.10a) represents a shift in the total energy, and will drop out of the problem once we perform optimisation.

Substituting (3.9) and (3.10a) into (2.13a), we have

$$\phi G_1'(c) + (1 - \phi)G_2'(c) - \frac{d^2c}{dx^2} = \mu, \quad \mu = \frac{\tilde{\mu}}{\Delta\tilde{G}}. \tag{3.11}$$

We may use the same analysis on (2.15a) to produce

$$G_1(c) - G_2(c) + WU'(\phi) - \lambda \frac{d^2\phi}{dx^2} = 0, \tag{3.12}$$

as long as U is differentiable at these points. However, the bulk values $\phi = 0$ and $\phi = 1$ are also critical points of the functional, since the derivative does not exist at these points.

In order to obtain values of the unknown parameters c_{\pm} and μ , we substitute $x = \pm\infty$ into (3.11) and (3.12):

$$G_1'(c_-) = \mu, \tag{3.13a}$$

$$G_2'(c_+) = \mu, \tag{3.13b}$$

$$G_1(c_-) - G_2(c_-) + WU'(1^-) = 0, \tag{3.14a}$$

$$G_1(c_+) - G_2(c_+) + WU'(0^+) = 0, \tag{3.14b}$$

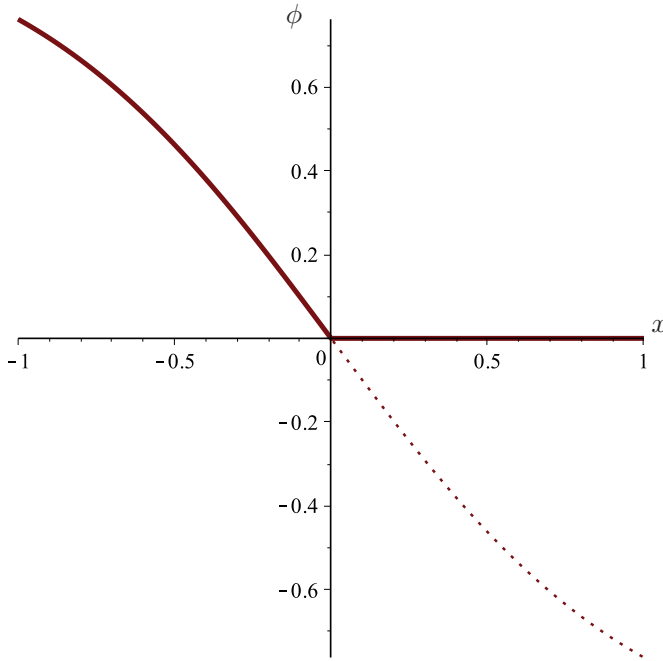


FIGURE 2. Schematic of the solution ϕ of (3.12). If the barrier did not exist (dotted curve in Figure 1), then ϕ would go negative (dotted curve). With the barrier, ϕ has compact support (solid curve). Here ϕ is taken to be 0 at $x = 0$ for simplicity.

where we have used (2.9) and (2.10). But if U' is smooth, (3.13) and (3.14) form an overdetermined system.

How do we resolve this? Consider a solution ϕ that approaches 0 given the potential in (3.4). As $\phi \rightarrow 0^+$, $U'(\phi) \rightarrow 1$, not zero. Hence the solution may not have $\phi' \rightarrow 0$ as $\phi \rightarrow 0^+$, which was implicit in the derivation of (3.14). This is because $\phi = 0$ is a steady state due only to the barrier. Hence, we expect that the solutions to (3.12) will have compact support (see Figure 2). However, note from (3.11) that c can still vary in the single-phase regions where $\phi = 0$ or $\phi = 1$, so c will not have compact support.

With our choice of f , the common tangent constraint (2.18) becomes

$$G'_1(c_-) = G'_2(c_+) = \frac{G_2(c_+) - G_1(c_-)}{c_+ - c_-} = \mu. \tag{3.15}$$

This set of equations determines $\{c_{\pm}, \mu\}$. An illustration of the common tangent constraint is shown in Figure 3. Here, the parameters used are

$$c_1^* = \frac{1}{2}, \quad c_2^* = \frac{3}{4}, \quad h_2 = 10, \tag{3.16a}$$

$$h_1 = 6. \tag{3.16b}$$

With this choice of parameters, the computed values of c_{\pm} are the following:

$$c_- = 0.634, \quad c_+ = 0.798. \tag{3.17}$$

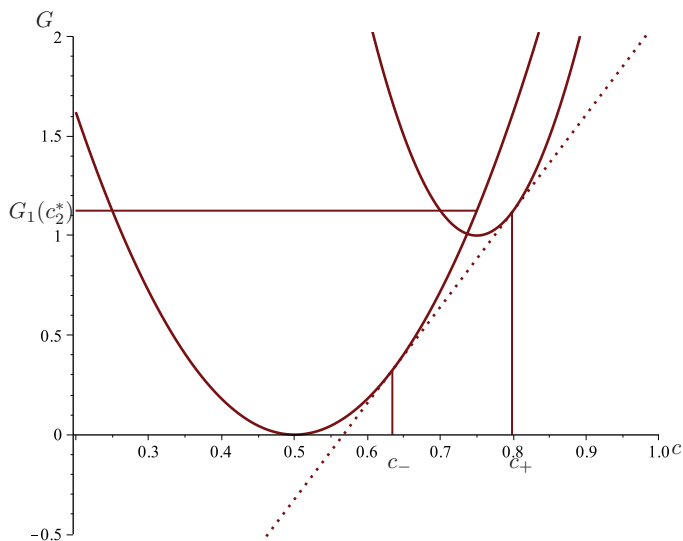


FIGURE 3. Two quadratic potentials (solid) and the common tangent (dotted): parameters as listed in (3.16).

4 Dividing the domain

Due to the form of the barrier function, ϕ can be identically equal to the extremal values 0 and 1 over various regions; therefore, we define x_l and x_r as follows:

$$\phi(x) = \begin{cases} 1, & x \leq x_l, \\ 0, & x \geq x_r. \end{cases} \tag{4.1}$$

Note that, x_l and x_r are unknown constants to be determined in the analysis. When $x > x_r$ or $x < x_l$, the U term in (3.10a) is zero, as is the $d\phi/dx$ term. Hence, in these regions the functional minimisation is done only over c . We call the region $x > x_r$ the *right exclusion zone*, and the region $x < x_l$ the *left exclusion zone*, where the terminology reminds us that ϕ will be excluded from the analysis in those regions.

Given the existence of the exclusion zones, we provide a schematic of the system in Figure 4. There are two ways to consider a system with such zones. The first (which we shall pursue here) is to treat the system as a free-boundary problem and derive appropriate boundary conditions at $x = x_l$ and $x = x_r$. The second is to use the principle of linear complementarity, as in [1].

In the left exclusion zone, the only governing equation is (3.11) with $\phi = 1$, the solution of which is

$$c_l(x) = c_1^* + \frac{\mu}{h_1^2} + A_1 \exp(h_1(x - x_l)), \quad x < x_l, \tag{4.2a}$$

where the subscript “l” indicates that we are in the left exclusion zone. Note from (4.2a) that

$$c_- = c_1^* + \frac{\mu}{h_1^2}, \tag{4.2b}$$

and that A_1 must be determined later.

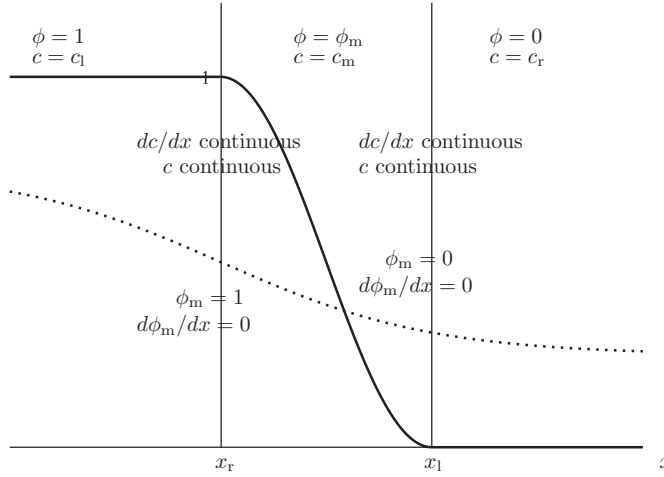


FIGURE 4. Schematic of subdivided diagram and characteristic sketches of ϕ (solid) and c (dotted).

Similarly, using (3.11) with $\phi = 0$ gives us the solution in the right exclusion zone:

$$c_r(x) = c_+ - A_r \exp(-h_2(x - x_r)), \quad x > x_r, \tag{4.3a}$$

$$c_+ = c_2^* + \frac{\mu}{h_2^2}. \tag{4.3b}$$

Note that by solving our system on a semi-infinite domain, we have significantly simplified the expressions in the exclusion zones.

Now we turn our attention to the mass constraint, rewritten in this context:

$$\lim_{L \rightarrow \infty} \frac{1}{2L} \left[\int_{-L}^{x_l} c_l(x) dx + \int_{x_l}^{x_r} c_m(x) dx + \int_{x_r}^L c_r(x) dx \right] = \bar{c}, \quad L = \tilde{L} \sqrt{\frac{\Delta \tilde{G}}{\kappa}}, \tag{4.4}$$

where we denote the solution in the transition region $x_l < x < x_r$ by c_m . The only terms that will contribute to the first and third integrals will be the constant terms in (4.2a) and (4.3a). But in that case the x_l and x_r terms would drop out, which is unreasonable since we expect their positions (and hence how much of each composition is in the solution) to matter.

To resolve the paradox, consider the finite domain $[-L, L]$. For a given value of L , we would expect particular values of x_l and x_r to characterise what fraction of the total mass comes from c_l , and what fraction comes from c_r . Now, double the length of the domain. Then to maintain the same fraction, we would have to double each of x_l and x_r . This suggests taking

$$x_l = \xi_l L, \quad x_r = \xi_r L; \quad -1 \leq \xi_l \leq \xi_r \leq 1, \tag{4.5}$$

where the ξ s are constant. But since the transition region must be finite, we must have that

$$x_r - x_l = \delta x \quad \implies \quad \xi_r = \xi_l + \frac{\delta x}{L}. \tag{4.6}$$

Therefore, we see that as $L \rightarrow \infty$, $\xi_1 \rightarrow \xi_r$. Also, the middle integral in (4.4) will be finite, and hence in the limit of large L will not contribute to the left-hand side.

Making these substitutions into (4.4), we have

$$\lim_{L \rightarrow \infty} \frac{1}{2L} \left[\int_{-L}^{\xi_1 L} c_1(x) dx + \int_{\xi_r L}^L c_r(x) dx \right] = \bar{c},$$

$$\lim_{L \rightarrow \infty} \frac{1}{2L} [c_-(\xi_1 L + L) + c_+(L - \xi_r L)] = \bar{c},$$

where we have used the fact that only the constant terms in c_1 and c_r will contribute to the expression once we divide by L and take the limit. Writing the common limit of ξ_1 and ξ_r as ξ_b , we obtain

$$\frac{c_-(\xi_b + 1) + c_+(1 - \xi_b)}{2} = \bar{c}, \tag{4.7}$$

which relates the interface position to the initial concentrations of the two bulk phases. Equation (4.7) is called the *lever rule*. Note that, ξ_b is directly related to the fraction of the ceramic in each phase. $\xi_b = -1$ corresponds to all c_1 , as expected. Similarly, all c_r corresponds to $\xi_b = 1$, and if $c_+ = c_-$, then $c_+ = c_- = \bar{c}$.

In order to solve our problem uniquely, we must specify the proper number of boundary conditions. There are seven constants to be determined. Six arise from the solutions of the ODEs (A_1 , A_r , and four more from the two second-order ODEs in the transition region). The last is the width δx of the transition zone (since the left endpoint is determined by the lever rule).

Equation (3.11) is smooth, so c and dc/dx must be continuous at $x = x_1$ and $x = x_r$, which yields four conditions. To find conditions on ϕ at these points, we note that since the energies in the exclusion zones must be minimised, we could pose a new optimisation problem just for $x_1 < x < x_r$, ignoring how those boundaries are determined. In that case, we would know nothing about ϕ on the boundaries *a priori*, and hence using the same techniques as in Section 2, we would have the natural boundary conditions

$$\frac{d\phi_m}{dx}(x_1) = 0, \tag{4.8a}$$

$$\frac{d\phi_m}{dx}(x_r) = 0, \tag{4.8b}$$

analogous to (2.15b). These conditions also appear in Blowey and Elliott [1]. However, consider how the free boundaries x_1 and x_r are defined: namely, that

$$\phi_m(x_1) = 1, \tag{4.9a}$$

$$\phi_m(x_r) = 0. \tag{4.9b}$$

Equations (4.8) and (4.9) provide four additional conditions, which then makes the system overdetermined.

To resolve this paradox, we evaluate the dimensionless form of (2.16) at x_1 and x_r :

$$G_2(c_+ - A_r) - G_1(c_- + A_1) - \mu[(c_+ - A_r) - (c_- + A_1)] - \left[\lambda \left(\frac{d\phi}{dx} \right)^2 + \left(\frac{dc}{dx} \right)^2 \right]_{x_1}^{x_r} = 0, \tag{4.10}$$

where we have used (3.10a), (4.2a), (4.3a), and (4.9). However, if we then integrate (3.11) across the left and right exclusion zones, we obtain

$$-G_1(c_- + A_1) + \mu(c_- + A_1) + \frac{1}{2} \left[\frac{dc_l}{dx}(x_l) \right]^2 = \mu c_- - G_1(c_-), \quad (4.11a)$$

$$G_2(c_+ - A_r) - \mu(c_+ - A_r) - \frac{1}{2} \left[\frac{dc_r}{dx}(x_r) \right]^2 = G_2(c_+) - \mu c_+. \quad (4.11b)$$

Substituting (4.11) into (4.10) and using (3.15), we obtain the following:

$$\left[\frac{d\phi}{dx}(x_l) \right]^2 = \left[\frac{d\phi}{dx}(x_r) \right]^2.$$

Hence the two conditions (4.8) are redundant. We then have only seven conditions to set our seven parameters, as required.

The final condition needed to close the system comes from the constraint (4.7), which follows directly from (2.12). Note that, it is this condition which keeps the system from being translationally invariant, as translating the solution will change the total mass.

5 Asymptotics: large internal barrier

Though straightforward in the exclusion zones, the system is substantially more complicated in (x_l, x_r) , since both (3.11) and (3.12) must be solved. Therefore, we examine the system in various asymptotic limits. We begin by considering the case where $W \rightarrow \infty$, which corresponds to a large internal maximum in the phase potential. In other words, there is a high energetic penalty for not being near the bulk phases $\phi = 0$ and $\phi = 1$. It is important to note that W is a parameter specific to this model, and hence is not known *a priori*; rather, it must be fit from experimental data.

In the rest of this manuscript we track only the leading-order terms, so we do not write our dependent variables in formal perturbation series. Taking $W \rightarrow \infty$, (3.12) becomes, to leading order,

$$U'(\phi_m) = 1 - 2\phi_m = 0,$$

which has the constant solution $\phi_m = 1/2$, which we expect to be unstable from the form of U . However, the formal verification of this has some later advantages.

The solution for ϕ_m has a discontinuity at $x = x_r$ which we resolve with the use of a boundary layer. Inserting the boundary layer, we let

$$X = W^{1/2}(x - x_r), \quad \Phi(X) = \phi_m(x). \quad (5.1)$$

This definition is equivalent to taking the characteristic length scale to be that associated with \tilde{W} instead of the one in (3.9). This makes sense, because the original length scale in (3.9) is associated with $\tilde{\kappa}$, which characterises variations in c . In contrast, \tilde{W} is associated with the potential for ϕ_m . Assuming that $W \rightarrow \infty$ is equivalent to saying the two processes occur on distinct length scales, and hence the equations decouple.

Substituting (5.1) into (3.12), we obtain, to leading order,

$$\lambda \frac{d^2\Phi}{dX^2} + 2\Phi = 1, \tag{5.2a}$$

$$\Phi(X) = \frac{1}{2} + A_s \sin X \sqrt{\frac{2}{\lambda}} + A_c \cos X \sqrt{\frac{2}{\lambda}}. \tag{5.2b}$$

But the solutions to the above equation oscillate, which cannot satisfy the matching condition

$$\Phi(X = -\infty) = \phi_m(x = x_r^-) = \frac{1}{2}.$$

Hence, we must conclude that there is no $O(1)$ region (x_l, x_r) where the unstable solution $\phi_m = 1/2$ holds. Therefore $x_l = x_r$, and we must insert an interior layer to smooth the jump in ϕ between 0 and 1. As we did in Section 4 with ξ , we denote the common limit of x_l and x_r by x_b .

We begin by finding the outer solution for c . As $W \rightarrow \infty$, the length scales separate. Hence ϕ totally drops out of the system on the x -scale. Instead, we have two solutions c_l and c_r which hold on two sides of some value $x = x_b$, determined by the lever rule (4.7). As noted above, both c and dc/dx will be continuous at $x = x_b$. Therefore, using (4.2a) and (4.3a), we obtain

$$c_l(x) = c_- + \frac{h_2(c_+ - c_-)}{h_2 + h_1} \exp(h_1(x - x_b)), \tag{5.3a}$$

$$c_r(x) = c_+ - \frac{h_1(c_+ - c_-)}{h_2 + h_1} \exp(-h_2(x - x_b)). \tag{5.3b}$$

We compare our analytic solutions with numerical simulations of the system. (See the Appendix for a discussion of the algorithm.) We use the parameters in (3.16) and (3.17), along with

$$L = 10, \quad \lambda = 1, \tag{5.4a}$$

$$W = 100. \tag{5.4b}$$

Moreover, for convenience we choose the value of \bar{c} in the lever rule (4.7) to force $x_b = 0$. The results are shown in Figure 5. Note the excellent agreement between the asymptotic and numerical results.

We now consider the solution in the boundary layer. For the reasons discussed in Section 3, we expect that $\Phi(X)$ will have compact support. Since the X problem is invariant under translation, we expect that $\Phi(X)$ will vary only in $(-X_b, X_b)$, where X_b is as yet undetermined. In particular, we have that the analogues to (4.8a) and (4.9) hold:

$$\frac{d\Phi}{dX}(-X_b) = 0, \tag{5.5a}$$

$$\Phi(-X_b) = 1, \quad \Phi(X_b) = 0. \tag{5.5b}$$

where we have used the fact that the equations in (4.8) are redundant.

Equation (5.2a) holds no matter the value of x_r , so (5.2b) still holds. Given that Φ is continuous at $X = \pm X_b$, equations (5.5) provide the boundary conditions on Φ needed to

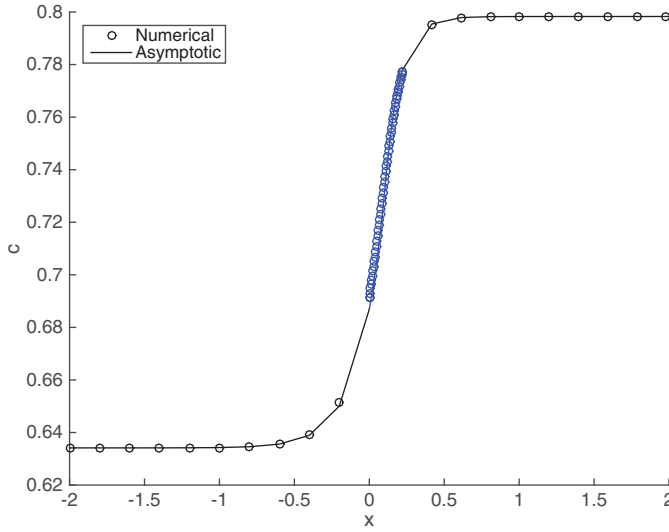


FIGURE 5. Plot of c [as given by (5.3)] versus x for the parameters in (3.16), (3.17), and (5.4). Note the smooth variation about $x_b = 0$. The transition region is indicated by the high density of simulation data points.

find the constants A . The solution is given by

$$\Phi(X) = \frac{1}{2} \left[1 - (-1)^n \sin \left(X \sqrt{\frac{2}{\lambda}} \right) \right], \quad |X| < X_b = \pi(n + 1/2) \sqrt{\frac{\lambda}{2}}, \quad n \geq 0, \quad (5.6)$$

where X_b is chosen to satisfy (5.5a). Hence, X_b plays the role of an eigenvalue in this problem.

From (5.6), we have an infinite number of solutions, two of which are shown in Figure 6. To select the physically appropriate one, we return to the free-energy formulation. The only portion of the free energy that depends on Φ is in the boundary layer:

$$\mathcal{F}_\Phi[\Phi] = \int_{-X_b}^{X_b} F \left(\Phi, \frac{d\Phi}{dX} \right) \frac{dX}{W^{1/2}}, \quad (5.7a)$$

where, to leading order in W , we have

$$F \left(\Phi, \frac{d\Phi}{dX} \right) \sim W \left[\Phi(1 - \Phi) + \frac{\lambda}{2} \left(\frac{d\Phi}{dX} \right)^2 \right]. \quad (5.7b)$$

Note that, these are exactly the terms that produced the operator in (5.2a).

Combining (5.6) and (5.7) and using our expression for X_b , we obtain

$$\mathcal{F}_\Phi[\Phi] \sim \frac{W^{1/2} \pi(n + 1/2)}{2} \sqrt{\frac{\lambda}{2}}. \quad (5.8)$$

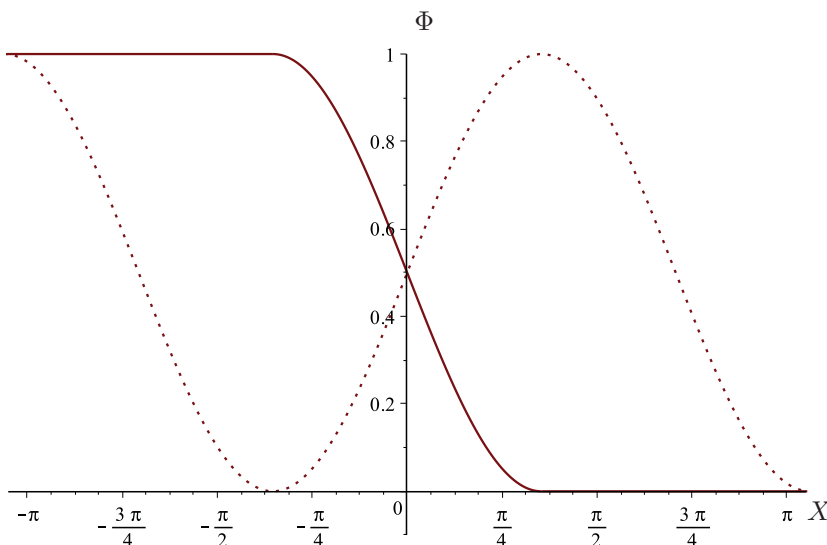


FIGURE 6. Graph of $\Phi(X)$ versus X . Solid curve: physical solution given by (5.9). Dotted curve: higher harmonic given by (5.6) with $n = 1$, which has unphysical oscillation.

Hence the minimising case has $n = 0$, and our final answer is

$$X_b = \frac{\pi}{2} \sqrt{\frac{\lambda}{2}}, \tag{5.9a}$$

$$\Phi(X) = \frac{1}{2} \left(1 - \sin X \sqrt{\frac{2}{\lambda}} \right), \quad |X| < \frac{\pi}{2} \sqrt{\frac{\lambda}{2}}. \tag{5.9b}$$

Figure 7 compares our analytical and numerical results. Note the excellent agreement.

As discussed above, in this asymptotic limit there is a separation of length scales associated with the transition regions for c and ϕ . In particular, c changes on the length scale associated with x , while ϕ changes on the much shorter length scale associated with X . This sort of scale separation has rarely, if ever, been seen in true experimental systems. Hence, while the limit that $W \rightarrow \infty$ simplifies the problem mathematically, in real physical systems W will remain $O(1)$.

6 Asymptotics: large free-energy concavity

Another asymptotic case of interest is when $h_x \rightarrow \infty$. This corresponds to one component whose free energy surface has high curvature, so it takes a lot of energy to displace c from c_x^* .

6.1 Large h_2

In the limit that $h_2 \rightarrow \infty$, the solution process in the exclusion zone is the same. Hence c_1 is still given by (4.2a), while c_r is given by (4.3a) in the limit of large h_2 :

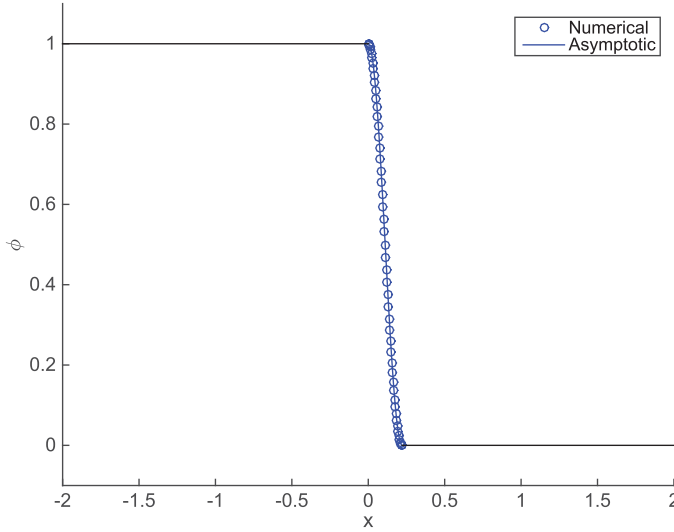


FIGURE 7. Plot of ϕ [as given by (5.9b)] versus x for the parameters in (3.16), (3.17), and (5.4). Note the sharp interface in ϕ in the transition region (indicated by the high density of simulation data points).

$$c_r(x) = c_+ = c_2^*, \quad x > x_r, \tag{6.1}$$

as one could expect physically from the high-curvature argument. In the transition region, (3.11) becomes

$$\phi_m G'_1(c_m) + (1 - \phi_m)h_2^2(c_m - c_2^*) - \frac{d^2c_m}{dx^2} = \mu, \tag{6.2}$$

where we have used (3.8b). The leading order of this equation for large h_2 is

$$c_m(x) = c_2^*, \tag{6.3}$$

and continuity of composition gives us

$$c_1(x) = c_- + (c_2^* - c_-) \exp(h_1(x - x_1)). \tag{6.4}$$

Moreover, substituting (6.1) into (4.7), we have the new lever rule

$$\frac{c_-(\zeta_b + 1) + c_2^*(1 - \zeta_b)}{2} = \bar{c}. \tag{6.5}$$

We cannot satisfy continuity of dc/dx at $x = x_1$, since the derivative of c_m is zero, which cannot match the derivative of the exponential c_1 . Therefore, a corner layer is needed near $x = x_1$, reflecting the fact that as $x \rightarrow x_1$, the $(1 - \phi_m)$ term in (6.2) becomes small enough to balance the h_2^2 term, allowing c_m to move away from c_2^* .

Before inserting the corner layer, we examine the behaviour of ϕ_m . Substituting (6.3) into (3.12), we obtain the following, to leading order:

$$\lambda \frac{d^2\phi_m}{dx^2} + 2W\phi_m = W + G_1(c_2^*) - 1, \tag{6.6a}$$

where we have used (3.8b). Solving (6.6a), we have

$$\phi_m(x) = \frac{1 + A_2}{2} + A_s \sin x \sqrt{\frac{2W}{\lambda}} + A_c \cos x \sqrt{\frac{2W}{\lambda}}, \quad A_2 = \frac{G_1(c_2^*) - 1}{W}, \quad (6.6b)$$

analogous to (5.2b).

In order to strengthen the analogy with the work in the previous section, we define the following quantities:

$$\bar{x} = \frac{x_l + x_r}{2}, \quad \Delta x = \frac{x_r - x_l}{2}, \quad x_m = x - \bar{x}. \quad (6.7)$$

Then our solution may be written as

$$\phi_m(x_m) = \frac{1 + A_2}{2} + A_s \sin x_m \sqrt{\frac{2W}{\lambda}} + A_c \cos x_m \sqrt{\frac{2W}{\lambda}}. \quad (6.8)$$

Since the interval is now $-\Delta x \leq x_m \leq \Delta x$, we may solve as in Section 4 with X replaced by x_m and X_b replaced by Δx . Thus, we have

$$\phi_m = \frac{1}{2} \left(1 - \frac{\sin x_m \sqrt{2W/\lambda}}{\sin \Delta x \sqrt{2W/\lambda}} \right) + \frac{A_2}{2} \left(1 - \frac{\cos x_m \sqrt{2W/\lambda}}{\cos \Delta x \sqrt{2W/\lambda}} \right), \quad |x_m| < \Delta x, \quad (6.9)$$

which satisfies (4.9).

In Section 4, the forcing constant was $1/2$, the mean of the matching values for ϕ , and hence we were able to satisfy both derivative conditions simultaneously. Here, we can satisfy only one of the conditions. Since we already expect a corner layer in c about $x = x_l$, we choose to satisfy the condition at $x = x_r$ ($x_m = \Delta x$) instead, yielding

$$\begin{aligned} \frac{d\phi_m}{dx_m}(\Delta x) &= -\frac{1}{2} \sqrt{\frac{2W}{\lambda}} \cot \left(\Delta x \sqrt{\frac{2W}{\lambda}} \right) + \frac{A_2}{2} \sqrt{\frac{2W}{\lambda}} \tan \left(\Delta x \sqrt{\frac{2W}{\lambda}} \right) = 0, \\ \cot^2 \left(\Delta x \sqrt{\frac{2W}{\lambda}} \right) &= A_2. \end{aligned} \quad (6.10)$$

Therefore, in order to satisfy the condition at $x_m = \Delta x$, we must have that $A_2 \geq 0$.

These computations are enough to determine our solutions except for a small corner layer near $x = x_l$, i.e., enough to determine the solution on a macroscopic scale. For mathematical completeness, we write down the equations in the corner layer. We let

$$X = h_2^A(x - x_l), \quad \phi_m(x_m) = 1 + h_2^{-A} \Phi(X), \quad c_m(x_m) = c_2^* + h_2^{-A} C(X), \quad (6.11)$$

where A is a constant that has to be chosen the same in each expression in order to make the derivatives match.

Substituting (6.11) into (3.11), we have that $A = 2/3$ and the leading order is given by

$$\Phi C + \frac{d^2 C}{dX^2} = 0. \quad (6.12)$$

Substituting (6.11) with $A = 2/3$ into (3.12), we obtain, to leading order,

$$\frac{C^2}{2} + \lambda \frac{d^2\Phi}{dX^2} = 0. \tag{6.13}$$

Equations (6.12) and (6.13) form a nonlinear system which can be solved numerically for the solutions in the boundary layer. From (6.13), we note that Φ should approach zero smoothly in this layer. Hence, Φ does not have compact support in X and the domain for X is fully infinite.

The boundary conditions for this system arise from matching to the outer solution, so we have

$$\begin{aligned} \frac{d\Phi}{dX}(-\infty) = 0, \quad \frac{dC}{dX}(-\infty) = \frac{dc_1}{dx}(x_1^-) = h_1(c_2^* - c_-), \\ \frac{dC}{dX}(\infty) = \frac{dc_m}{dx_m}(-\Delta x^+) = 0, \quad \frac{d\Phi}{dX}(\infty) = \frac{d\phi_m}{dx_m}(-\Delta x^+) = -\sqrt{\frac{2WA_2}{\lambda}}, \end{aligned}$$

where we have used (6.9) and (6.10).

6.2 Large h_1

For numerical computations, it is better to examine the case of $h_1 \rightarrow \infty$, as described in the Appendix. This case is largely similar to the case where $h_2 \rightarrow \infty$; we summarise the differences below.

Here, it is the left state which is trapped near c_1^* , so we have

$$c_l(x) = c_- = c_1^*, \quad x < x_1; \quad c_m(x) = c_1^*, \tag{6.14a}$$

analogous to (6.1) and (6.3). Continuity then yields

$$c_r(x) = c_+ - (c_+ - c_1^*) \exp(-h_2(x - x_r)), \tag{6.14b}$$

analogous to (6.4). Moreover, substituting (6.14a) into (4.7), we have the new lever rule

$$\frac{c_1^*(\xi_1 + 1) + c_+(1 - \xi_1)}{2} = \bar{c}. \tag{6.15}$$

A graph of our solutions is shown in Figure 8. We use the parameters in (3.16a) and (5.4a); however, we replace the parameters in (3.16b) and (5.4b) with

$$h_1 = 63, \quad W = 1 \quad \implies \quad c_- = 0.501, \quad c_+ = 0.787, \tag{6.16a}$$

$$A_1 = 4.125, \quad \Delta x = 0.324. \tag{6.16b}$$

We have taken $W = O(1)$ in accordance with our discussion at the end of Section 5. As expected, the outer solution matches the computed solution for most of the regime, but a corner layer is needed to smooth the derivative. In that region, the change in $c = O(h_1^{2/3}) \approx 6.3 \times 10^{-2}$, which is roughly the size of the deviation shown in the graph.

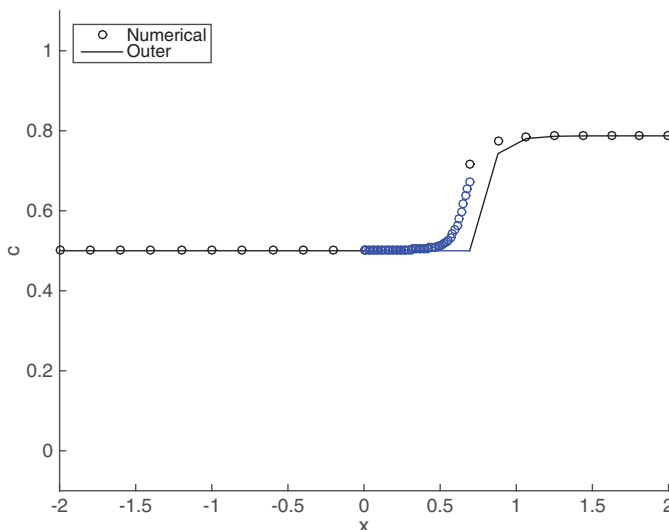


FIGURE 8. Plot of c [as given by (6.14a)] versus x for the parameters in (3.16a), (5.4a), and (6.16). Note the kink in the graph at $x = x_r$. The transition region is indicated by the high density of simulation data points.

In the transition region, the analogue to (6.6a) is

$$\lambda \frac{d^2 \phi_m}{dx^2} + 2W \phi_m = W - G_2(c_1^*).$$

In this case, it is convenient to change the sign of the A parameter, so we write the solution as

$$\phi_m(x_m) = \frac{1}{2} \left(1 - \frac{\sin x_m \sqrt{2W/\lambda}}{\sin \Delta x \sqrt{2W/\lambda}} \right) - \frac{A_1}{2} \left(1 - \frac{\cos x_m \sqrt{2W/\lambda}}{\cos \Delta x \sqrt{2W/\lambda}} \right), \quad |x_m| < \Delta x, \quad (6.17a)$$

$$A_1 = \frac{G_2(c_1^*)}{W}, \quad (6.17b)$$

analogous to (6.9). A graph of our solutions is shown in Figure 9. Note that, here we have a much closer agreement between the analytical and numerical solutions.

The corner layer is now about $x = x_r$, and Δx is given by (6.10) with A_2 replaced by A_1 ; moreover, the appropriate scalings are

$$X = h_1^{2/3}(x - x_r), \quad \phi_m(x_m) = h_1^{-2/3} \Phi(X), \quad c_m(x_m) = c_1^* - h_1^{-2/3} C(X), \quad (6.18)$$

which yield (6.12) and (6.13). Thus, the underlying structure of the corner layer remains the same, whether the layer is on the left or the right. It is just the scalings and the sign of the dependent variables that change. The same is true of the boundary conditions, which

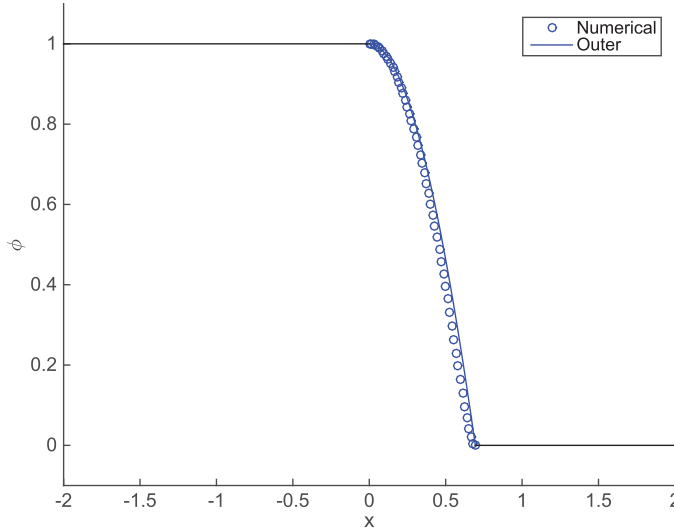


FIGURE 9. Plot of ϕ [as given by (6.17)] versus x for the parameters in (3.16a), (5.4a), and (6.16a). The transition region is indicated by the high density of simulation data points.

remain of the same form, but with slightly different constants to reflect the new case:

$$\begin{aligned} \frac{d\Phi}{dX}(\infty) &= 0, & \frac{dC}{dX}(\infty) &= -\frac{dc_r}{dx}(x_r^+) = h_2(c_+ - c_1^*), \\ \frac{dC}{dX}(-\infty) &= -\frac{dc_m}{dx_m}(\Delta x^-) = 0, & \frac{d\Phi}{dX}(-\infty) &= -\frac{d\phi_m}{dx_m}(\Delta x^-) = \sqrt{\frac{2WA_1}{\lambda}}. \end{aligned}$$

Figures 8 and 9 illustrate that in this regime, we find the physically observed case where both the composition and phase vary on the same length scale. Moreover, the free energy of a material can be measured independently and hence is not a characteristic of this model; therefore it is quite possible to find materials exhibiting this behaviour.

7 Conclusions

Oxide ceramics have become widely used in many industries in recent years. Hence, it is important for scientists and engineers to have good models for their internal microstructure. Such insights will lead to better designed and more efficient filters, heat shields, and other devices.

In this work, we extended a phase-field model of Wheeler *et al.* [10, 11] in two ways. First, we extended the domain to a fully infinite one for algebraic convenience. Second, we introduced an obstacle (infinite barrier) potential in the portion of the energy potential associated with the phase. This type of potential forces the bulk phase distribution to remain pinned at the desired values 0 and 1, even under the imposition of a separate external field. Once the model is postulated, the mathematical problem reduces to a minimisation problem over all possible states.

The introduction of such a potential introduces several mathematical complications. Because of the lack of differentiability of the potential, the solutions for the phase

composition have compact support. This introduces two *exclusion zones* where the phase composition is fixed at its bulk value, but the concentrations are not. In those regions, the concentration decays exponentially from the value at the exclusion zone interface to its far-field value. The placement of the exclusion zone interfaces is largely determined by the lever rule (4.7).

The mathematical system to be solved in the transition region between the two exclusion zones is quite complicated, and in the general case must be tackled numerically. Fortunately, in several experimentally useful cases, asymptotics can provide analytical expressions for key variables of interest.

The first case we considered was that of large W , which corresponds to a high internal maximum in the phase portion of the potential. The equation for the phase Φ becomes an eigenvalue problem in the transition zone; only the first eigenfunction is physically allowable due to energy minimisation considerations. In this case, the composition varies on an $O(1)$ length scale, but the transition zone for the phase Φ becomes infinitesimal [width $O(W^{-1/2})$]. This separation of scales is not typically seen in experiments; so this mathematical simplification is unphysical. Hence when fitting experimental data, we would expect that $W = O(1)$.

The second case we considered was that of large curvature in one of the bulk free energy densities, corresponding to the case where it takes a lot of energy to displace the concentration from its local minimum. In that case, the transition region for both quantities is the same, as typically seen in experiments. However, there are discontinuities in the derivatives of both the concentration and the phase distribution at one transition interface. These discontinuities force the introduction of a corner layer [width $O(h_x^{-2/3})$], where a system of two coupled nonlinear second-order ODEs must be solved.

Our work on the internal microstructure of the transition regions supplements the traditional work on the bulk phases. As such, it should be useful to scientists and engineers when working to optimise the design of oxide ceramics.

Acknowledgements

This work was supported in part by NSF grant DMS-1261592. The authors thank Daniel Anderson of George Mason University and Leslie Button of Corning for helpful discussions regarding this manuscript, as well as the reviewer for constructive suggestions.

Nomenclature

Units are listed in terms of mass (M), moles (N), length (L), and time (T). If a symbol appears both with and without tildes, the symbol with tildes has units, while the one without is dimensionless. Equation numbers where a variable is first defined are listed, if appropriate.

- A : arbitrary constant, variously defined.
- $C(X)$: corner-layer concentration variable (6.11).
- $c(\tilde{\mathbf{x}})$: composition fraction at position $\tilde{\mathbf{x}}$ (2.1).
- $\tilde{\mathcal{F}}[\tilde{c}, \tilde{\phi}]$: free energy, units ML^2/T^2 (2.8).
- \tilde{F} : free energy density, units ML/T^2 (2.11b).
- $\tilde{f}(\tilde{c}, \tilde{\phi})$: bulk free energy density, units ML/T^2 (2.5).

- $\tilde{\mathcal{G}}[c, \phi]$: function to be minimised including constraint, units ML/T^2 .
 $\tilde{G}_\alpha(\tilde{c})$: “bulk” free energy density of phase α , units ML/T^2 (3.1).
 H : conserved constant (2.16).
 \tilde{h} : constant in definition of free energy density, units ML/T^2 (3.3).
 i : integer used to index composition (2.1).
 j : integer used to index composition (2.6).
 \tilde{L} : dummy length used to normalise domain, units L (2.11a).
 M : number of phases (2.3).
 N : number of compositions (2.1).
 $\tilde{U}(\vec{\phi})$: phase potential, units ML/T^2 (3.2).
 \tilde{V} : arbitrary volume, units L^3 (2.8).
 \tilde{W} : constant characterising the potential, units ML/T^2 (3.4).
 X : boundary-layer variable, variously defined (5.1).
 \tilde{x} : position in oxide ceramic units L (2.1).
 \tilde{x} : distance along ceramic, units L (2.11a).
 y : scaled variable used in numerical simulation (A 1).
 z : dependent variable used in numerical simulation (A 2).
 α : integer used to index composition (2.3).
 β : integer used to index composition (2.7).
 $\Delta\tilde{G}$: difference between energy minima of phases (3.7).
 Δx : half-width of transition region in case of large h_x (6.7).
 δx : width of transition region (4.6).
 $\tilde{\kappa}$: gradient energy coefficient associated with the compositions, units ML^3/T^2 (2.6).
 $\tilde{\lambda}$: gradient energy coefficient associated with the phases, units ML^3/T^2 (2.7).
 $\tilde{\mu}$: Lagrange multiplier, units ML/T^2 .
 ζ : scaling factor for subdomains (4.5).
 $\Phi(X)$: phase fraction in the boundary layer (5.1).
 $\phi(\tilde{x})$: phase fraction at position \tilde{x} (2.3).
 ψ : test function for variational problem.

Other notation

- b : as a subscript, used to indicate the shared boundary of the exclusion zones (4.7).
 c : as a subscript on A , used to indicate the coefficient of a cosine function (5.2b).
 l : as a subscript, used to indicate the left exclusion zone (4.1).
 m : as a subscript, used to indicate the solution in the transition region (4.4).
 r : as a subscript, used to indicate the right exclusion zone (4.1).
 s : as a subscript on A , used to indicate the coefficient of a sine function (5.2b).
 ϵ : as a subscript on U , used to indicate smoothed potentials (3.5).
 Φ : as a subscript on \mathcal{F} , used to indicate that portion of the free energy that depends on Φ (5.7a).
 $-$: as a subscript, used to indicate a value as $x \rightarrow -\infty$ (2.10).

- + : as a subscript, used to indicate a value as $x \rightarrow \infty$ (2.10).
 * : as a superscript, used to indicate a minimum in the bulk free energy density (3.3).
 - : used to indicate a spatial average (2.12).

References

- [1] BLOWEY, J. & ELLIOTT, C. (1991) The Cahn-Hilliard gradient theory for phase separation with non-smooth free energy. Part I: Mathematical analysis. *Eur. J. Appl. Math.* **2**, 233–280.
 [2] BROWN, J. & SOBSEY, M. D. (2009) Ceramic media amended with metal oxide for the capture of viruses in drinking water. *Env. Tech.* **30**(4), 379–391.
 [3] COGSWELL, D. A. & CARTER, W. C. (2011) Thermodynamic phase-field model for microstructure with multiple components and phases: The possibility of metastable phases. *Phys. Rev. E* **83**(6, 1), 061602.
 [4] GRASHCHENKOV, D. V., BALINOVA, Y. A. & TINYAKOVA, E. V. (2012) Aluminum oxide ceramic fibers and materials based on them. *Glass Ceram.* **69**(3–4), 130–133.
 [5] HEULENS, J., BLANPAIN, B. & MOELANS, N. (2011) A phase field model for isothermal crystallization of oxide melts. *Acta Mater.* **59**, 2156–2165.
 [6] KEANE, M. (2003) Ceramics for catalysis. *J. Math. Sci.* **38**(23), 4661–4675.
 [7] KIM, I. J. (2010) Thermal stability of Al_2TiO_5 ceramics for new diesel particulate filter applications—a literature review. *J. Ceram. Proc. Res.* **11**(4), 411–418.
 [8] NACKEN, M., HEIDENREICH, S., HACKEL, M. & SCHAUB, G. (2007) Catalytic activation of ceramic filter elements for combined particle separation, NO_x removal and VOC total oxidation. *Appl. Catal. B* **70**(1–4), 370–376.
 [9] WEI, G. C., LAPATOVICH, W. P., BROWNE, J. & SNELGROVE, R. (2008) Dysprosium oxide ceramic arc tube for HID lamps. *J. Phys. D* **41**(14).
 [10] WHEELER, A. A., BOETTINGER, W. & MCFADDEN, G. (1992) Phase-field model for isothermal phase transitions in binary alloys. *Phys. Rev. A* **45**, 7424–7439.
 [11] WHEELER, A. A., BOETTINGER, W. & MCFADDEN, G. (1993) Phase-field model for solute trapping during solidification. *Phys. Rev. E* **47**, 1893–1909.

Appendix A Numerical solutions

In the transition zone, we solve the problem numerically to compare with our asymptotic solutions. As indicated in Section 4, the width δx of the transition zone is unknown and plays the role of an eigenvalue. By introducing the variable

$$y = \frac{x - x_1}{\delta x}, \quad (\text{A } 1)$$

the transition zone becomes the fixed interval $0 \leq y \leq 1$ and δx appears as an unknown coefficient in the problem. We use the Matlab `bvp5c` function, which works only on a first-order system. Therefore, by defining a vector \mathbf{z} as follows:

$$\mathbf{z} = \left(c_m, \frac{dc_m}{dy}, \phi_m, \frac{d\phi_m}{dy} \right), \quad (\text{A } 2)$$

our system (3.11) and (3.12) becomes the following:

$$\frac{dz_1}{dy} = z_2, \quad (\text{A } 3a)$$

$$\frac{dz_2}{dy} = -(\delta x)^2 [\mu - z_3 h_1^2 (z_1 - c_1^*) - (1 - z_3) h_2^2 (z_1 - c_2^*)], \quad (\text{A } 3b)$$

$$\frac{dz_3}{dy} = z_4, \quad (\text{A } 3c)$$

$$\frac{dz_4}{dy} = \frac{(\delta x)^2}{\lambda} \left\{ \frac{h_1^2 (z_1 - c_1^*)^2}{2} - \left[1 + \frac{h_2^2 (z_1 - c_2^*)^2}{2} \right] + W(1 - 2z_3) \right\}, \quad (\text{A } 3d)$$

subject to the boundary conditions

$$z_3(0) - 1 = 0, \quad z_4(0) = 0, \quad z_3(1) = 0, \quad (\text{A } 4)$$

which come from (4.8a) and (4.9), and the additional conditions

$$h_1[z_1(0) - c_-] - \frac{z_2(0)}{\delta x} = 0, \quad (\text{A } 5a)$$

$$h_2[z_1(1) - c_+] + \frac{z_2(1)}{\delta x} = 0, \quad (\text{A } 5b)$$

which come from matching the transition-region solution to (4.2a) and (4.3a).

bvp5c requires an initial guess for our parameters and functions. For ϕ_m , we use (5.9b), while for c_m , we use a tanh function to connect the solutions in the exclusion zones smoothly:

$$c_m(y) = \frac{c_+ + c_-}{2} + \frac{c_+ - c_-}{2} \tanh(y - 1/2). \quad (\text{A } 6)$$

Lastly, we assume that $\delta x = 2$. The procedure iterates until convergence, which is quite quick in the large- W case. In the case of large h_2 , the procedure fails to converge for h_2 larger than about 20. The case of large h_1 is more stable (perhaps due to the vagaries of how the algorithm refines its internal mesh), though $h_1 = 63$ is the maximum integral value that converged.